The Nature of CISK in a Generalized Continuous Model

BIN WANG*

Geophysical Fluid Dynamics Program, Princeton University, Princeton, NJ 08542

(Manuscript received 14 April 1986; in final form 19 November 1986)

ABSTRACT

In spite of the fundamental difficulties in interpreting the growth of tropical storms, the basic idea of CISK remains valuable in understanding the instability resulting from the interaction between cumulus convection and large-scale flows. A generalized solution of a quasi-balanced continuous model, which can be applied to various types of vertical heating distribution and basic-state stratification, is derived and used to explore the behaviors of the CISK mode.

In the absence of cumulus momentum mixing, the CISK solution exhibits, in general, a scale selection. However, two types of unbounded growth rates associated with different closure assumptions may exist. Both of them take place in a common situation that is characterized by local warming at the top of the moist convergence layer in the area of rising motion. In these circumstances, the direct coupling between the heating and the large-scale moisture supply through the divergent wind component dominates over the indirect coupling through the rotational component. It is suggested that, for a feasible Ekman CISK mechanism, the dominant feedback of the convective heating to the low-level moisture convergence must be of an indirect nature. In this feedback process, planetary vorticity and/or preexisting relative vorticity play an essential role in converting heating-induced divergent kinetic energy to rotational kinetic energy, thus accelerating the spin-up of a large-scale vortex.

The cumulus momentum mixing destabilizes short waves by enhancing cyclonic circulation at the top of the Ekman layer and by reducing the vertical extent of the temperature disturbance; meanwhile, it stabilizes long waves by weakening the anticyclonic circulation in the upper levels.

1. Introduction

a. *Applicability of the CISK theory to real atmospheric phenomena*

The CISK (Conditional Instability of the Second Kind) theory was originally proposed to explain the growth of tropical cyclones (Ooyama, 1964; Charney and Eliassen, 1964). Charney and Eliassen (referred to hereafter as CE) initiated a prototypical model to demonstrate a possibility for the growth of tropical cyclones by cooperative interaction between cumulus convection and synoptic disturbances. Although the model results compare favorably to observations in some aspects, such as energetics and vertical structures, the linear CISK theory has faced some fundamental difficulties in explaining tropical cyclogenesis. First, the balance assumption adopted in CE's model is a severe restriction on the theory's tropical application. The CISK mechanism requires a preexisting disturbance of small amplitude possessing positive low-level vorticity or convergence within a fixed region. Since the effect of the Earth's rotation is weak in low latitudes, for a balance assumption to be justified the preexisting disturbance must already have fairly strong vorticity (Ooyama, 1982). In low latitudes, the validity of Charney and Eliassen's (1949) Ekman formula, which was derived for a steady, quasi-geostrophic flow with uniform stratification, is also questionable unless the vortex itself is strong. In view of this restriction, the CISK theory does not explain the genesis of tropical storms. Second, without including a nonlinear inertial term, a linear theory is unable to explain the typical scale of the intense tropical cyclones, which is the radius of the maximum wind (Ooyama, 1982). Lastly, although the mean tropical atmosphere is unstable in the undiluted ascent of moist air in the boundary layer, it is not necessarily unstable in highly dilute real clouds. The preexisting ambient convective available potential energy is obviously insufficient to produce an intense storm. Emanuel (1986) shows that the maintenance, and possibly the intensification, of tropical storms depends exclusively on heat transfer from the ocean. These weaknesses and deficiencies depreciate the scientific value of tropical CISK.

One may, however, appreciate the basic idea of CISK in a broader context. In his 1982 paper, Ooyama stated that he views CISK in terms of the conceptual content that has grown and matured with advances in modeling work; thus, the spirit of CISK as the cooperative intensification theory is valid and alive (Ooyama, 1982).

* Present affiliation: Department of Meteorology, University of Hawaii, Honolulu, HI 96822.

From a broader point of view, the advance of the CISK theory may be regarded as the earliest effort at understanding the dynamic and thermodynamic interactions between cumulus convection and large-scale disturbance. Such interaction, if it exists, is not just confined to the tropics. Cumulus heating also represents an important source of energy and plays an essential role in the dynamics of some subtropical and extratropical weather systems, such as extratropical cyclones (Tracton, 1973; Smith et al., 1984), monsoon depression (Krishnamurti et al., 1976), polar lows (Rasmussen, 1979; Sardie and Warner, 1983), explosive cyclones (Gyakum, 1983), a heavy rainfall vortex (Chen and Dell'Osso, 1984), and Tibetan Plateau vortices (Yeh, 1979; Dell'Osso and Chen, 1986).

A recent study of a heavy rain vortex that formed over the eastern flank of the Tibetan Plateau (Wang and Orlanski, 1987) indicates that the vortex originated and rapidly developed in a stagnation region on the lee side of the plateau, where both vertical and horizontal shears are vanishingly small. Numerical experiments show that, without latent heating, the dynamic instability and/or forcing of large-scale flow interacting with the plateau is not sufficient to generate the observed vortex. On the other hand, the blocking effect of the plateau favors the establishment of a conditionally unstable environment. The simulation with latent heating (in terms of an explicit scheme) indicates that a sudden onset of vigorous deep convection followed by a rapid vorticity intensification at 700 mb took place once the dynamic forcing associated with a meso-α scale plateau disturbance was positioned over the western stagnation region. The principal result of this study suggests that the warm, heavy rain vortex in this case study is basically driven by cumulus convective heating. Another example is the warm low-level vortices that form over the main body of the Tibetan Plateau in the rainy season (referred to here as plateau vortices). The monthly mean sounding in July at 1200 UTC (1800 LST) from Lhasa, which is representative of conditions over the central plateau where plateau vortices most frequently occur, shows that the atmosphere is in a convectively unstable state, the lifting condensation level is around 540 mb, and the region of positive buoyancy extends from 500 to 170 mb (Yeh, 1979; Wang, 1987a). One of the prominent synoptic features is that the generation of plateau vortices is often accompanied by appreciable amounts of convective precipitation (on average, 6–11 mm day^{-1}; see Lu et al., 1984). Numerical experiments performed by Dell'Osso and Chen (1986) and Wang (1987a) demonstrate that condensational latent heating is a primary energy source.

For these disturbances driven primarily by convective heating, a key problem is how the latent heat released in the cumulus clouds can be employed to provide energy for growth in the synoptic or subsynoptic scales. The larger-scale destabilization with respect to deep moist convection appears to enhance cumulus activity. Thus, a self-exciting system (Emanuel, 1983) through feedback of latent heat release becomes quite possible. This is the essence of CISK. It is important to note that, in the middle latitudes or subtropical regions, the presence of stronger planetary vorticity makes the quasi-geostrophic (or balance) assumption justifiable and Charney and Eliassen's (1949) expression for Ekman pumping acceptable. In addition, the nonlinearity and the surface energy flux are not crucial in explaining their development because these midlatitude disturbances (e.g., the heavy rain vortex and the plateau vortices) are much weaker in circulation and much shorter in duration (1–2 days) in comparison with the tropical storms. They have also well-defined characteristic dimensions of meso-α scale (several hundred to one thousand kilometers). A linear instability resulting from cooperative interaction between convection and quasi-geostrophic flow seems to be applicable to these nonmaritime events.

In his analysis of the *genesis* of tropical cyclones, Ooyama (1982) suggested that at the beginning of the genesis process, moist convection is modulated and sustained by a *mesoscale system,* which is in between the cumulus convection and quasi-horizontal balanced flow in the tropics. However, Ooyama also realized the different situations in the midlatitudes, saying that "in the extratropics, on the other hand, the scale separation between the mesoscale and the synoptic scale is small, suggesting a closer control of the former by the latter." In the cases of the meso-α scale heavy rain vortex and the plateau warm vortex, the assumption that the rate of heating can be parameterized in terms of the subsynoptic-scale convergence of moisture is more acceptable than in the tropics. That assumption constitutes the basis of the present heating parameterization, which was remotely related to Kuo's (1974) scheme in the present study by introducing two additional assumptions. This simple parameterization was also derived using moisture and heat budget arguments (Stevens and Lindzen, 1978; Emanuel, 1983). The use of this simple scheme provides meaningful insight into the nature of the interaction between cumulus convection and synoptic flow and into the roles convective heating plays in the development of synoptic-scale disturbances (e.g., Mak, 1982; Sardie and Warner, 1983; Moorthi and Arakawa, 1985; Wang and Barcilon, 1986; Bannon, 1986; Wang, 1987a).

b. *Objectives*

Although the simple scheme of the cumulus parameterization has achieved some successes, it is subject to a number of assumptions and hypotheses, and some deficiencies are related to the limitations caused by the simplification. A most serious controversy has remained as to the applicability of the CISK growth rate to the initial selection mechanism of the disturbances.

In this regard, the unstable mode in CE's model has two deficiencies: 1) the curve of the growth rate levels off at short wavelengths, and no characteristic scale of the instability is actually found; 2) the growth rate becomes unbounded at certain middle wavelengths as heating intensity exceeds some critical value. Similar drawbacks, e.g., the growth rate increases monotonically with decreasing wavelength, also appear in other model studies using a similar cumulus parameterization. In the past two decades there have been a large number of researchers who explored the nature of CISK and attempted to account for the causes of the deficiencies encountered in CISK models (e.g., Charney, 1973; Chang and Williams, 1974; Davies and de Guzman, 1979; Mak, 1981; Pedersen and Rasmussen, 1985).

In general, CISK solutions are rather sensitive to the partitioning of the heat of condensation among the model layers and to the vertical variation of the static stability of the basic state (e.g., Syōno and Yamasaki, 1966) and are also significantly affected by the way in which the equations are differenced (Koss, 1976). Therefore, a model with continuous vertical structure is better suited for theoretical study of CISK.

In section 2, theoretical parameterization of the effects of both cumulus heating and momentum mixing is reviewed and a vertically continuous model is formulated. The model assumes that large-scale moisture supply concentrates in a surface moist layer, the top of which is treated as an independent parameter that can be either at or above the top of the Ekman boundary layer. A generalized CISK solution, which can be applied to various types of continuous basic state stratification and vertical heating distribution, is derived in section 3. The behavior of the generalized solution is discussed in section 4. A particular effort is made to reveal the physical causes responsible for the unbounded growth rate by verifying the CISK hypothesis against its closure assumptions.

In addition to the thermodynamic influence, cumulus convection also contributes to vertical exchange of horizontal momentum. Stevens et al. (1977) suggested the substantial importance of cumulus momentum mixing in interpreting the structure of large-scale tropical wave disturbances. During the past decade or so, an increasing number of studies have been made to diagnose the bulk effects of cumulus momentum transport in tropical weather systems (cyclones, cloud clusters and easterly waves). The majority of those investigations appear to confirm the significance of the dynamic impact of cumulus momentum transport on larger-scale motions. However, our knowledge of the dynamic influences of cumulus momentum transport on CISK-induced disturbances is rather limited. Section 5 treats this problem, where the effect of downgradient momentum mixing and cloud mass detrainment on CISK is qualitatively assessed through numerical solutions.

2. A continuous CISK model with cumulus momentum mixing

The CISK theories assume that the horizontal scales of large-scale rotational flow and cumulus convection are well separated, so that any quantity, I, can be expressed as $I = \langle I \rangle + I'$, where $\langle I \rangle$ denotes averaged large-scale quantity and I' the fluctuation that is caused by convection. The area used in averaging is determined by a characteristic length scale, such that the spatial variation of the large-scale system can be well resolved, whereas the collective effect of the cumulus-scale motion can be described statistically.

Kuo (1974) showed that the average vertical transport of horizontal momentum by subgrid convection can be written as

$$\langle \omega' \mathbf{v}' \rangle = \frac{\delta}{1-\delta}(\omega_c - \langle \omega \rangle)(\mathbf{v}_c - \langle \mathbf{v} \rangle),$$

where δ is fractional area occupied by active cumulus clouds, $\langle \omega \rangle$ and $\langle \mathbf{v} \rangle$ stand for large-scale vertical and horizontal velocities, and ω_c and $\mathbf{v}_c$ stand for the mean vertical and horizontal velocities of the whole active clouds, respectively. If one further assumes that $\delta \ll 1$ and $\omega_c \gg \langle \omega \rangle$, and defines total cloud mass flux by $M_c = \delta \omega_c$, the Reynolds stress due to the vertical exchange of horizontal momentum by cumulus convection can be expressed by

$$-\frac{\partial}{\partial p}\langle \omega' \mathbf{v}' \rangle = \frac{\partial}{\partial p}[M_c(\langle \mathbf{v} \rangle - \mathbf{v}_c)]. \tag{2.1}$$

The horizontal transport of momentum by cumulus clouds will be neglected, since the cumulus flux of momentum is mainly in the vertical direction. Schneider and Lindzen (1976) derived an expression equivalent to (2.1) and referred to it as cumulus friction. They also pointed out that, if the major contribution of the cumulus convection to the momentum budget comes from deep clouds and if the environmental vertical shear is weak, the cumulus clouds will *conserve* approximately their momentum due to their large velocity. The assumption that the mean cloud velocity, $\mathbf{v}_c$, equals the large-scale velocity at the cloud base, $\langle \mathbf{v}_b \rangle$, leads to the expression

$$-\frac{\partial}{\partial p}\langle \omega' \mathbf{v}' \rangle = M_c \frac{\partial \langle \mathbf{v} \rangle}{\partial p} + \frac{\partial M_c}{\partial p}(\langle \mathbf{v} \rangle - \langle \mathbf{v}_b \rangle), \tag{2.2}$$

which is equivalent to the formulation proposed by Ooyama (1971). The first term on the right-hand side of (2.2) points to the diffusive nature of the vertical mixing of the momentum by cumulus clouds. Some recent diagnostic studies of cloud clusters (Tollerud and Esbensen, 1983) and of tropical cyclones (Lee, 1984) suggest that the vertical momentum redistribution acts to reduce the midlevel cyclonic winds and the upper-level anticyclonic winds as well, indicating the relevance of the downgradient mixing for those

disturbances. The second term on the right-hand side of (2.2) reflects the impact of the detrained cumulus momentum. It was considered to be particularly responsible for the reduction of the anticyclonic circulation at the upper troposphere around 200 mb (Sui and Yanai, 1986). Equation (2.2) is probably the simplest parameterization that describes the essential mechanisms by which the cumulus-scale motion influences the large-scale horizontal momentum.

The parameterized cumulus condensation heating on the large-scale flow is assumed to be represented by

$$\langle Q_c \rangle = -\tilde{\alpha} L_c \bar{q} \omega(p_m) \eta(p), \tag{2.3a}$$

where L_c is the latent heat of condensation, and $\bar{q}$ is the mean specific humidity in the moist convergence layer, the top of which is at p_m. The quantity $\tilde{\alpha}$ is a nondimensional coefficient proportional to the ratio of the convective precipitation to the total amount of moisture that converges into the cumulus cloud ensemble. When the convective precipitation is relatively strong, the value of $\tilde{\alpha}$ should be close to unity. For convenience, $\tilde{\alpha}$ will be assigned a value of unity. The quantity $\eta(p)$ is a specified, *nondimensional* function describing the vertical distribution of heat and must satisfy

$$\int_0^1 \eta(p) dp = 1, \tag{2.3b}$$

where p is nondimensional pressure. The essence of the heating parameterization, (2.3), was discussed by Wang and Barcilon (1986). In the present model, we shall omit diabatic heating other than cumulus latent heat and take turbulent viscosity into account only via Ekman layer dynamics.

The hydrostatic perturbation motion, linearized about a basic state at rest on f-plane (x, y, p, t) coordinates, is governed by the following vorticity and divergence equations and the first law of thermodynamics:

$$\left.\begin{aligned} &\frac{\partial \zeta}{\partial t} - \frac{\partial \omega}{\partial p} + \mathrm{Ro}\frac{\partial}{\partial p}[M_c(\zeta(p_b) - \zeta)] = 0 \\ &\mathrm{Ro}^2\left\{\frac{\partial \zeta}{\partial t} + \frac{\partial \omega}{\partial p} + \mathrm{Ro}\frac{\partial}{\partial p}\left[M_c\left(\frac{\partial \omega}{\partial p}(p_b) - \frac{\partial \omega}{\partial p}\right)\right]\right\} \\ &\qquad + \zeta - \nabla^2\phi = 0 \\ &\frac{\partial}{\partial t}\frac{\partial \phi}{\partial p} + S(p)\omega = \epsilon\frac{\eta(p)}{p}\omega(p_m) \end{aligned}\right\}, \tag{2.4}$$

where the hydrostatic relation and the continuity equation, along with Eqs. (2.2) and (2.3a), have been exploited. The quantities ζ, ϕ and ω are the vertical component of the vorticity, geopotential height and vertical p-velocity, respectively. The function $S(p)$ is the static stability parameter. In the linear system (2.4), $M_c(p)$ represents *zonally averaged* total cumulus cloud mass flux and is a function of pressure only. All quantities in (2.4) have been nondimensionalized by

$$p^* = P_0 p, (x^*, y^*) = L(x, y),$$

$$t^* = (L/V)t, \phi^* = f_0 L V \phi,$$

$$(\omega^*, M_c^*) = \frac{P_0 V^2}{f_0 L^2}(\omega, M_c), S^* = f_0^2 L^2 P_0^{-2} S,$$

where f_0 is a constant Coriolis parameter; P_0, L, V, and L/V are the basic scales for the pressure, horizontal length, horizontal velocity, and time, respectively. The asterisks indicate the corresponding dimensional quantities in (2.4). The nondimensional numbers appearing in (2.4) are

$$\mathrm{Ro} = \frac{V}{f_0 L}, \quad \text{the Rossby number,} \tag{2.5a}$$

$$\epsilon = \tilde{q}\frac{L_c R}{f_0 L^2 C_p^2}, \quad \text{the coefficient of heating intensity,} \tag{2.5b}$$

where R is the gas constant, and C_p is the specific heat of the air at constant pressure. We now focus our attention on the perturbation motion that is characterized by $\mathrm{Ro}^2 \ll 1$, for which the terms less than or equal to $O(\mathrm{Ro}^2)$ can be omitted and the quasi-geostrophic balance is approximately valid. We shall refer to it as the dynamically large-scale motion. For the case of interest here the heating intensity coefficient, ϵ, is of order unity, implying that the primary effect of the cumulus convection on the large-scale motion is the release of latent heat; whereas the cumulus friction, that is O(Ro), has secondary influence on the large-scale motion.

For the dynamically large-scale flow, the nondimensional governing equations (2.4) then reduce to

$$\frac{\partial}{\partial t}\nabla^2\phi - \frac{\partial \omega}{\partial p} + \mathrm{Ro}\frac{\partial}{\partial p}[M_c(p)(\nabla^2\phi_b - \nabla^2\phi)] = 0, \tag{2.6a}$$

$$\frac{\partial}{\partial t}\frac{\partial \phi}{\partial p} + S(p)\omega = \epsilon\frac{\eta(p)}{p}\omega_m, \tag{2.6b}$$

where $\phi_b \equiv \phi(p_b)$, $\omega_m \equiv \omega(p_m)$. The model atmosphere is vertically continuous and is confined between $p = p_u$ (the upper boundary) and $p = p_e$ (the lower boundary), where p_e refers to the pressure at the top of the Ekman layer. The nondimensional boundary conditions are assumed to be given by

$$\omega = 0, \quad \text{at} \quad p = p_u, \tag{2.7a}$$

$$\omega = -r\nabla^2\phi, \quad \text{at} \quad p = p_e, \tag{2.7b}$$

where

$$r = \frac{\rho_e g L}{P_0 V}\left(\frac{A_z f_0}{2}\right)^{1/2} \tag{2.8}$$

measures the strength of the Ekman layer pumping, ρ_e the density at $p = p_e$, and A_z the vertical turbulent viscosity in the Ekman layer. Equation (2.7b) states

that the interior vertical velocity at p_e matches the vertical velocity induced by the Ekman layer pumping; the latter is similar to that derived by Charney and Eliassen (1949).

The crucial part of the above formulation is the linearized treatment of the bulk effect of cumulus convection. Both the cumulus heating and the friction are essentially nonlinear. The neglect of the nonlinear cumulus stress term in the horizontal momentum equation, i.e., $-\partial/\partial p[M'_b(\langle \mathbf{v}_b \rangle - \mathbf{v}')]$, is actually not justified. However, since our knowledge of the impact of the cumulus momentum transport on CISK is extremely limited, it seems to be helpful to identify its possible qualitative influences first within the framework of linear dynamics. The implications and validity of using an unconditional heating were discussed by a number of authors (e.g., Davies and de Guzman, 1979; Wang, 1987b).

3. Generalized CISK solution

If we first examine the lowest order problem, namely, neglect the O(Ro) terms, Eqs. (2.6a) and (2.6b) can be combined into a single equation for vertical p-velocity ω, and the lower boundary condition (2.7b) can also be expressed solely in terms of ω. We further seek exponentially growing solutions of the form

$$\omega(x,p,t) = \mathrm{Re}\{\Omega(p)e^{i(kx-\sigma t)}\}.$$

The vertical structure function, $\Omega(p)$, growth rate, $\sigma_i \equiv \mathrm{Im}(\sigma)$, and propagation speed, $\mathrm{Re}(\sigma)/k$, are determined by solving the following eigenvalue problem:

$$\frac{d^2\Omega}{dp^2} - k^2 S(p)\Omega = -\epsilon k^2 \frac{\eta(p)}{p}\Omega(p_m), \tag{3.1}$$

$$\Omega = 0, \quad \text{at} \quad p = p_u, \tag{3.2a}$$

$$\sigma\Omega + ir\frac{d\Omega}{dp} = 0, \quad \text{at} \quad p = p_e, \tag{3.2b}$$

where stratification, $S(p)$, and heating function, $\eta(p)$, are assumed to be continuous in the model domain, $p_u \leqslant p \leqslant p_e$.

Using the method of solution described by Wang and Barcilon (1986), one may obtain a generalized CISK solution for a class of basic flows with various types of stratification, $S(p)$, and heating function, $\eta(p)$. Assuming that $\Omega_1(p)$ and $\Omega_2(p)$ are two complementary solutions of Eq. (3.1), one may construct

$$f_1(p) \equiv \sigma A(p) + irB(p), \tag{3.3}$$

$$I_2(p) \equiv \int_{p_t}^{p} \frac{\eta(t)}{t} \frac{\Omega_2(p_u)\Omega_1(t) - \Omega_1(p_u)\Omega_2(t)}{\Omega_1'(t)\Omega_2(t) - \Omega_2'(t)\Omega_1(t)}\,dt, \tag{3.4}$$

where p_t is the pressure at the cloud top,

$$A(p) = \Omega_1(p_e)\Omega_2(p) - \Omega_2(p_e)\Omega_1(p), \tag{3.5a}$$

$$B(p) = \Omega_1'(p_e)\Omega_2(p) - \Omega_2'(p_e)\Omega_1(p), \tag{3.5b}$$

and the prime denotes the derivative with respect to p. For the situation in which the top of the moist convergence layer is located at or below the cloud base, p_b, i.e., $p_m \geqslant p_b$, the dispersion equation can be written as

$$f_1(p_u) - \epsilon k^2 f_1(p_m) I_2(p_b) = 0,$$

which yields

$$\sigma = ir\frac{\epsilon k^2 B(p_m) I_2(p_b) - B(p_u)}{A(p_u) - \epsilon k^2 A(p_m) I_2(p_b)}, \quad (p_b \leqslant p_m). \tag{3.6}$$

The solution for the case in which $p_m < p_b$ is relegated to the Appendix.

The real functions, $A(p)$ and $B(p)$, which are linear combinations of the complementary solutions, $\Omega_1(p)$ and $\Omega_2(p)$, are determined by the basic-state stratification, $S(p)$, and the real function, $I_2(p)$, must be determined by both the basic-state stratification, $S(p)$, and the cumulus heating function, $\eta(p)$.

Three specialized stratification profiles are considered; for convenience, they are labeled SP1, SP2 and SP3 (see Table 1). Profile SP1 depicts a model atmosphere with constant density; profiles SP2 and SP3 represent, respectively, non-Boussinesq model atmospheres with a constant temperature and with a constant lapse rate, $-\partial T/\partial z$. The variable S_0 is the static stability parameter at sea level. In general, the stratification calculated from observed temperature profile (e.g., Rosenthal, 1978) can be well approximated by both SP3 and SP2.

Also listed in Table 1 are the two complementary solutions, $\Omega_1(p)$ and $\Omega_2(p)$, as well as $A(p)$ and $B(p)$, for the three specialized stratifications. For models SP1 and SP2, it is apparent that

$$A(p) \geqslant 0, \tag{3.7a}$$

$$B(p) > 0. \tag{3.7b}$$

The equal sign in (3.7a) holds only when $p = p_e$, i.e., $A(p)$ vanishes only at the model's lower boundary, where $p = p_e$. For model SP3, the numerical calculation verifies the validity of (3.7a,b).

To simulate various types of vertical heating distribution, we specify a general heating function, defined by

$$\eta(p) = \begin{cases} 0, & p < p_t \quad \text{or} \quad p > p_b, \\ \tilde{A}[a(p_1 - p)(p - p_t)^2 + (1-a)(p_1 - p)^2(p - p_t)], & \\ & p_t \leqslant p \leqslant p_b, \end{cases} \tag{3.8a}$$

where the coefficient $\tilde{A}$, which satisfies (2.3b), is

$$\tilde{A} = \left\{ \frac{1-2a}{4}(p_b^4 - p_t^4) + \frac{1}{3}[3a(p_1 + p_t) - 2p_1 - p_t] \times (p_b^3 - p_t^3) + \frac{1}{2}[p_1(p_1 + 2p_t) - a(p_1^2 + p_t^2 + 4p_1 p_t)] \times (p_b^2 - p_t^2) + p_1 p_t[a(p_1 + p_t) - p_1](p_b - p_t) \right\}^{-1}. \tag{3.8b}$$

TABLE 1. The complementary solutions of Eq. (3.1), $\Omega_1(p)$ and $\Omega_2(p)$, and functions $A(p)$ and $B(p)$ defined by (3.5a, b) for three model stratifications. $J_\nu(x)$ denotes νth order Bessel function, $\Gamma(\nu)$ represents the Gamma function, and the prime represents the derivative with respect to p.

Model	Stratification $S(p)$	Complementary solutions $\Omega_1(p)$ and $\Omega_2(p)$	$A(p)$	$B(p)$
SP1	$\bar{S}$	$\frac{1}{2}e^{\mu p}$, $\frac{1}{2}e^{-\mu p}$ $\mu \equiv k\bar{S}^{1/2}$	$sh\mu(p_e - p) \geq 0$	$\mu ch\mu(p_e - p) > 0$
SP2	$\frac{S_0}{p^2}$	$p^{1/2+b}$, $p^{1/2-b}$ $b \equiv (\frac{1}{4} + k^2 S_0)^{1/2}$	$\sqrt{pp_e}\left[\left(\frac{p_e^b}{p}\right) - \left(\frac{p^b}{p_e}\right)\right] \geq 0$	$\left(\frac{p}{p_e}\right)^{1/2}\left[\left(\frac{1}{2}+b\right)\left(\frac{p_e^b}{p}\right) - \left(\frac{1}{2}-b\right)\left(\frac{p^b}{p_e}\right)\right] > 0$
	$\frac{S_0}{p^{2-m}}$	$p^{1/2}J_\nu(\mu p^{m/2})$	$p_e R_\nu(p_e) R_{-\nu}(p_e)$	$R_\nu(p_e)R'_{-\nu}(p_e) + p_e R'_\nu(p_e)R_\nu(p)$
SP3	$m \equiv \frac{R}{g}\left(-\frac{\partial T}{\partial z}\right)$	$p^{1/2}J_{-\nu}(\mu p^{m/2})$	$-pR_\nu(p) - R_{-\nu}(p_e) \geq 0$	$-pR\nu(p)R'_{-\nu}(p_e) > 0$
	$\nu = \frac{1}{m}$	$\mu = -\frac{2iS_0^{1/2}}{m}k$	$R_\nu(p) = \sum_{k=0}^{\infty} \frac{(-\mu^2 p^m/4)^k}{k!\Gamma(\nu+k+1)}$	

In (3.8a,b) a and p_1 are two adjustable shape parameters. Changing a from 0 to 1 shifts the location of the maximum heating continuously from the upper part to the lower part of the cloud (Fig. 1a). The condition $p_1 = p_b$ implies that the heating vanishes at the cloud base. When $p_1 > p_b$ ($p_1 < p_b$), there is a heating (cooling) at the cloud base (Fig. 1b). Figure 1c shows the nondimensional heating distribution functions for Yanai et al.'s (1973) profile and for Johnson's (1984) profile for the partitioned cumulus component. It is seen that, if one chooses $a = 0.4$ and $p_1 = 0.97$, then the $\eta(p)$ profile given by (3.8a) is rather close to Yanai's profile, while an η-profile with $a = 1.0$ and $p_1 = 0.93$ can approximate Johnson's profile quite well.

With heating profile (3.8a) and stratification SP2, one can derive the following expression for $I_2(p_b)$:

$$I_2(p_b) = p_u^{0.5-b}\tilde{I}_2(p_b; b) + p_u^{0.5+b}\tilde{I}_2(p_b; -b), \quad (3.9a)$$

where $b = (\frac{1}{4} + S_0k^2)^{1/2}$ and

$$\tilde{I}_2(p_b; b) = -\frac{\tilde{A}}{2b}\left\{(2a-1)\left[\frac{p_b^{3.5+b} - p_t^{3.5+b}}{3.5+b} - \frac{(p_1+p_t)}{2.5+b}\right.\right.$$
$$\times (p_b^{2.5+b} - p_t^{2.5+b}) + \left.\frac{p_1 p_t}{2.5+b}(p_b^{2.5+b} - p_t^{2.5+b})\right]$$
$$+ [p_1 - a(p_1+p_t)]\left[\frac{p_b^{2.5+b} - p_t^{2.5+b}}{2.5+b} - \frac{(p_1+p_t)}{1.5+b}\right.$$
$$\left.\left.\times (p_b^{1.5+b} - p_t^{1.5+b}) + \frac{p_1 p_t}{0.5+b}(p_b^{.5+b} - p_t^{.5+b})\right]\right\}. \quad (3.9b)$$

The quantity $I_2(p_b)$ in (3.6) represents the contribution of cumulus heating to the growth of the CISK modes. The numerical computations indicate that, as long as latent heat is released in a vertically integrated sense, $I_2(p_b)$ is always positive for all wavenumbers. The properties pertaining to the signs of $A(p)$, $B(p)$ and $I_2(p_b)$ are useful for the discussions below.

4. The scale selection of CISK

The solution (3.6) indicates that quasi-geostrophic CISK possesses a unique unstable mode. In the absence of cumulus heating, this mode would decay at a rate

$$\sigma_i = -rB(p_u)/A(p_u). \quad (4.1)$$

(For convenience, a negative growth rate is hereafter referred to as a damping rate.) In the presence of cumulus heating, the release of latent heat may cause amplification of this mode. The characteristics of the instability depend crucially upon the closure assumptions used in the parameterization scheme.

a. Closure assumption of type 1: $p_m = p_e$

In his closure of the balanced model for the tropical cyclones, Ooyama (1964, 1969) assumed that the release of latent heat by moist convection in a vertical column was proportional to the supply of unstable moist air at the top of the mixed boundary layer. When this closure assumption is applied to (3.6), i.e., p_m is set to equal p_e, the growth rate of the CISK mode becomes

$$\sigma_i = \sigma_i^{(1)} + \sigma_i^{(2)} = \frac{r}{A(p_u)}[\epsilon k^2 B(p_m) I_2(p_b) - B(p_u)]. \quad (4.2)$$

Solution (4.2) clearly shows the dual role the Ekman pumping plays in CISK. On the one hand, it damps the vorticity disturbance via vortex compressing (stretching) in the positive (negative) vorticity region; the second term on the right-hand side of (4.2), $\sigma_i^{(2)}$, measures this damping rate, which is identical to that given by (4.1) for the *adiabatic* case. On the other hand, the Ekman pumping provides water vapor convergence; hence it sustains cumulus convection, which releases latent heat in the positive vorticity region and contributes to the generation of eddy available potential

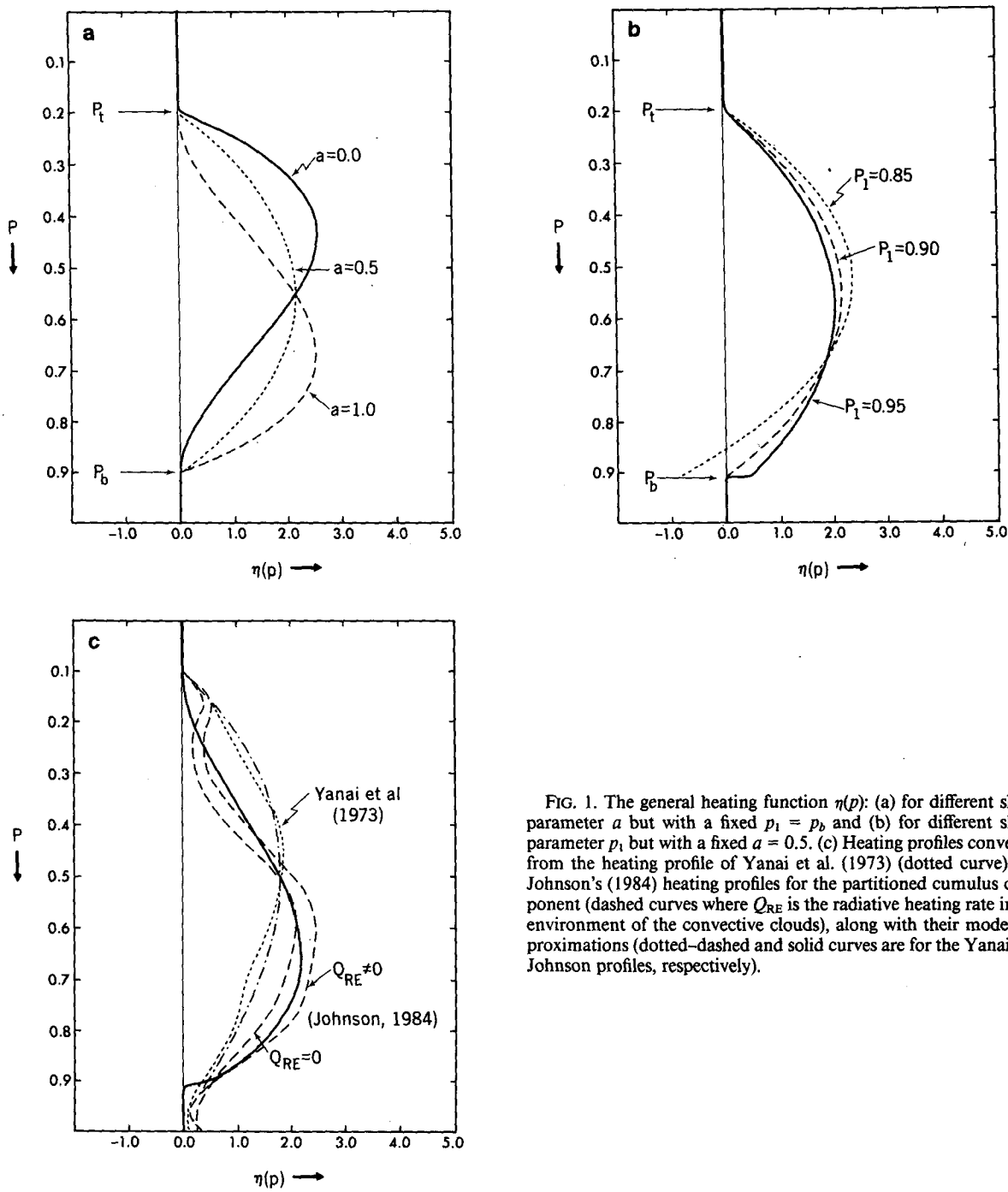

FIG. 1. The general heating function $\eta(p)$: (a) for different shape parameter a but with a fixed $p_t = p_b$ and (b) for different shape parameter p_t but with a fixed $a = 0.5$. (c) Heating profiles converted from the heating profile of Yanai et al. (1973) (dotted curve) and Johnson's (1984) heating profiles for the partitioned cumulus component (dashed curves where Q_{RE} is the radiative heating rate in the environment of the convective clouds), along with their model approximations (dotted–dashed and solid curves are for the Yanai and Johnson profiles, respectively).

energy. The first term on the right-hand side of (4.2), $\sigma_i^{(1)}$, expresses this growth rate, which is proportional to the heating intensity. The amplification of a CISK disturbance can only occur when the contribution of the Ekman pumping to the genesis of eddy available potential energy dominates the Ekman dissipation of eddy kinetic energy or when the heating intensity, ϵ (or the mean specific humidity, $\bar{q}$), exceeds a critical value, ϵ_c (or $\bar{q}_c$), where

$$\epsilon_c = \frac{B(p_u)}{k^2 B(p_m) I_2(p_b)}, \quad \bar{q}_c = \epsilon_c \frac{f_0^2 L^2 C_p}{L_c R}. \tag{4.3}$$

The CISK threshold, ϵ_c, depends on the wavenumber, the Coriolis parameter, the basic-state stratification and the vertical heat distribution, but does not depend upon the intensity of the Ekman layer viscosity, A_z, although the growth rate is invariably proportional to r or to the square root of A_z.

In their analysis of a continuous model with a specified heating profile, Chang and Williams (1974) showed that the contribution to the growth rate due to diabatic heating is proportional to $k^2/(\pi^2/2 + 2k^2)$, while the decay rate due to the Ekman dissipation is proportional to $-k/(1 - 1/(2k))$. Therefore, they concluded that for small scales the unbounded Ekman damping rate will always dominate, and the short-wave cutoff is inherent in their model.

We now consider a model with a representative stratification, SP2, and with a general heating profile, (3.8). Substituting the expressions for $A(p)$ and $B(p)$ given in Table 1 and the expression for $I_2(p_b)$ given by (3.9a) into (4.2), one can show that for small scales (large wavenumber) the damping rate, $\sigma_i^{(2)}$, in (4.2) is

$$\sigma_i^{(2)} = -r\frac{B(p_u)}{A(p_u)} \to -\frac{r}{p_e} S_0^{1/2} k, \quad \text{as} \quad k \to \infty.$$

The growth rate due to cumulus heating, $\sigma_i^{(1)}$, in (4.2) becomes

$$\sigma_i^{(1)} = r\epsilon k^2 \frac{B(p_m)}{A(p_u)} I_2(p_b) \to rkS_0^{1/2}\epsilon\eta(p_e)\left(\frac{p_b}{p_e}\right)^{b+0.5},$$

$$\text{as} \quad k \to \infty,$$

where $b = (1/4 - S_0k^2)^{1/2}$. Note that the magnitude of $\sigma_i^{(1)}$ crucially depends upon the *heating condition* at the top of the Ekman layer. If there is no diabatic heating at the top of the Ekman layer, i.e., $\eta(p_e) = 0$, then $\sigma_i^{(1)}$ approaches zero and the total growth rate approaches $-rS_0^{1/2}k/p_e$ for short waves. Thus a short-wave cutoff and wave selection are warranted. However, if $p_b = p_e$ and $\eta(p_e) \neq 0$,

$$\sigma_i^{(1)} \to rS_0^{1/2}\epsilon\eta(p_e)k, \quad \text{as} \quad k \to \infty,$$

indicating that the absolute value of $\sigma_i^{(1)}$ increases linearly with increasing wavenumber, k, but its sign depends on the sign of $\eta(p_e)$. In the presence of diabatic cooling ($\eta(p_e) < 0$) at the top of the Ekman layer, $\sigma_i^{(1)}$ goes to $-\infty$ and the short CISK mode decays even faster than the adiabatic mode. This situation is possible if the net evaporation takes place near the cloud base in the presence of falling precipitation and evaporatively driven downdrafts. On the other hand, the presence of the diabatic heating at the top of the Ekman layer makes $\sigma_i^{(1)}$ monotonically increase with decreasing wavelength and the total growth rate

$$\sigma_i = \sigma_i^{(1)} + \sigma_i^{(2)} \to rS_0^{1/2}\left[\epsilon\eta(p_e) - \frac{S_0}{p_e}\right]k, \quad \text{as} \quad k \to \infty,$$

demonstrating that it changes from a large decay rate to a large growth rate for short waves when heating intensity, $\epsilon\eta(p_e)$, increases from a value smaller than S_0/p_e to a value greater than S_0/p_e. Thus the short-wave blowup (i.e., the monotonic increase in the growth rate with decreasing wavelength) occurs when

$$\epsilon\eta(p_e) > \frac{S_0}{p_e}. \tag{4.4}$$

The physical implication of this can be understood in terms of the lower boundary condition (3.2b), from which

$$-\left.\frac{d\Omega}{dp}\right|_{p=p_e} = \frac{\sigma_i}{r}\Omega(p_e).$$

Using the continuity equation and (4.2), one obtains

$$D(p_e) = \frac{\omega(p_e)}{A(p_u)}[\epsilon k^2 B(p_m) I_2(p_b) - B(p_u)],$$

where $D(p_e)$ stands for horizontal divergence at the top of the boundary layer, p_e. For short waves, i.e., as $k \to \infty$,

$$D(p_e) \to S_0^{1/2} k p_e \left[\epsilon\frac{\eta(p_e)}{p_e} - \frac{S_0}{p_e^2}\right]\omega(p_e). \tag{4.5}$$

Equation (4.5) shows that the moisture convergence at p_e is determined by the competitive effects between the convective heating at p_e (the first term on the right-hand side) and the adiabatic cooling due to the Ekman pumping-induced ascending motion, $\omega(p_e)$. The criterion (4.4), therefore, implies that the short-wave blowup takes place when the effect of the convective heating exceeds that of the Ekman pumping-induced cooling. From an alternative point of view, the criterion (4.4) also implies a local warming at the top of the boundary layer in the area of rising motion.

Growth rates have been computed for a particular set of model parameters in a reference run, which are listed in Table 2. Figure 2 shows the variations of growth rate in units of day^{-1}, with wavenumber k and $\bar{q}^*$ calculated from the reference run using the stratification profile, SP2, and the heating profile, (3.8). For the reference run, the moisture that converges into the clouds comes from below cloud base, and diabatic heating vanishes at the top of the Ekman layer, so the short-wave cutoff is guaranteed. The solid curve that corresponds to Eq. (4.3) (the 0-contour in Fig. 2) divides an unstable region above from a stable region below. We note that this threshold curve has a minimum at an intermediate wavelength. This minimum threshold moisture content indicates the minimum moisture content required for CISK and represents an important characteristic of CISK. In terms of a continuous CISK model with a constant heating profile, it has been shown that the minimum threshold of CISK basically depends on only the vertical distributions of the temperature and moisture of the basic state (Wang, 1987b).

In multilayer models such as used in Koss (1976), the short-wave cutoff is evident only when the vertical heating distribution shows peak values in the upper levels. In the present continuous model, however, the short-wave cutoff still exists even when the maximum of the heating occurs in the low levels (Fig. 2). This is a noticeable difference between the layer and contin-

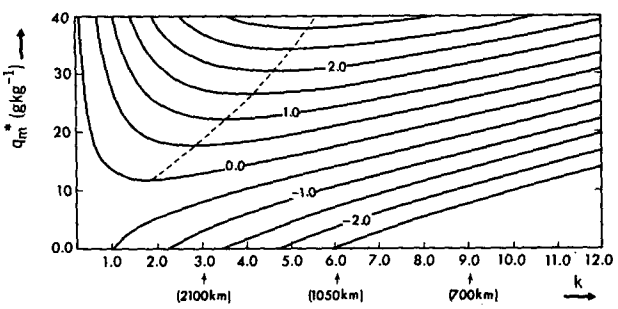

FIG. 2. Plot of contours of the growth rate in day^{-1} as functions of nondimensional wavenumber, k, and specific humidity of the moist boundary layer, q_m^*, for the reference run. The dimensional wavelengths corresponding to $k = 3.0$, 6.0 and 9.0 are given. The dashed curve indicates the most unstable modes.

uous models. Pederson and Rasmussen (1985) showed that the lack of the short-wave cutoff in a number of layer models is either induced by an erroneous use of the thermodynamic equation, as pointed out by Chang and Williams (1974), or caused by an inconsistent use of the vorticity equation on the top of the Ekman layer. They also used a Boussinesq continuous model and demonstrated, in terms of the leading term, the close relationship between the short-wave cutoff and the heating on the top of the Ekman layer. The present analysis confirms and extends their result in a more general continuous model.

b. *Closure assumption of type 2: $p_m < p_e$*

In CE's model, the convective heating was estimated from the total column moisture convergence. As a result, a part of the heating was proportional to the vertical velocity at the interior levels. This closure assumption assumed that cumulus heating is not solely controlled by the Ekman layer pumping, but also by the diabatic heating. Thus, it is dynamically similar to the case where $p_m < p_e$ in the present continuous model; i.e., the top of the moist convergence layer is located above the Ekman layer, so that the water vapor convergence is affected directly by the diabatic heating. Under this assumption the growth rate is given by (3.6), and the CISK threshold ϵ_c is given by (4.3). It is obvious from (3.6) that, when

$$\epsilon = \epsilon_b = \frac{A(p_u)}{k^2 A(p_m) I_2(p_b)}, \tag{4.6}$$

the growth rate approaches infinity at a certain middle wavelength, a feature that appears in CE's model when heating intensity exceeds a critical value.

To discuss the implication of (4.6), it is convenient to consider a simple model with a constant stratification and with a heating function

$$\eta(p) = \begin{cases} 0, & p < p_t \quad \text{and} \quad p > p_b, \\ Ap, & p_t \leq p \leq p_b = p_m. \end{cases}$$

With these specifications, (4.6) becomes

$$\epsilon = \frac{\bar{S}}{A} \frac{\sinh(\mu p_e - \mu p_u)}{\sinh(\mu p_e - \mu p_m)[\cosh(\mu p_b - \mu p_u) - \cosh(\mu p_t - \mu p_u)]} > \frac{\bar{S}}{A}, \tag{4.7}$$

since the quantity in the square bracket is larger than unity for any $\mu = \bar{S}^{1/2}k$. From the thermodynamic equation applied at the top of the moist layer, where $p = p_m$, i.e.,

$$\frac{\partial}{\partial t}\left(\frac{\partial \phi}{\partial p}\right)\bigg|_{p=p_m} = (-\bar{S} + \epsilon A)\omega(p_m),$$

we observe that condition (4.7) implies that there is an increase in the temperature at the top of the moist convergence layer in an ascending region, because the adiabatic cooling due to ascending motion cannot compensate the convective heating in situ at p_m. Therefore, the condition for the growth rate blowup at a finite wavelength, (4.6), has essentially the same meaning as implied by the short-wave blowup condition, (4.4).

Figure 3a sketches the instability diagram for the case where $p_m (= p_b = p_t) < p_e$ by using the model with the stratification, SP2, and with the heating function, (3.8). All the parameters take the values listed for the reference run except p_m, p_b and p_t. Note that, with this parameter setting, the top of the moist convergence layer extends above the Ekman layer ($p_m < p_e$); however, there is no diabatic heating at the cloud base, since $p_m = p_b = p_t$. The top and bottom solid curves in Fig. 3a correspond, respectively, to the blowup mode given by (4.6) and the neutral mode given by (4.3) for

TABLE 2. List of the model parameters used for the reference run. All quantities are dimensional except the shape parameters, a and p_t.

	Model parameters	Values in the reference run
f_0	Coriolis parameter (s^{-1})	0.377×10^{-4}
A_z	eddy viscosity coefficient (m^2 s^{-2})	10
S_0	static stability parameter at 1000 mb (m^2 s^{-2} mb^{-2})	0.01
$\bar{q}$	mean specific humidity in the moist layer (g kg^{-1})	20
p_m	pressure at the top of the moist convergence layer (mb)	900
p_e	pressure at the top of the Ekman layer (mb)	900
p_b	pressure at cloud base (mb)	900
p_t	pressure at cloud top (mb)	200
p_u	pressure at the upper boundary (mb)	100
a	shape parameter	1.0
p_1	shape parameter	0.9
ρ_e	density at p_e (kg m^{-3})	1.20
γ	averaged lapse rate (K m^{-1})	0.0

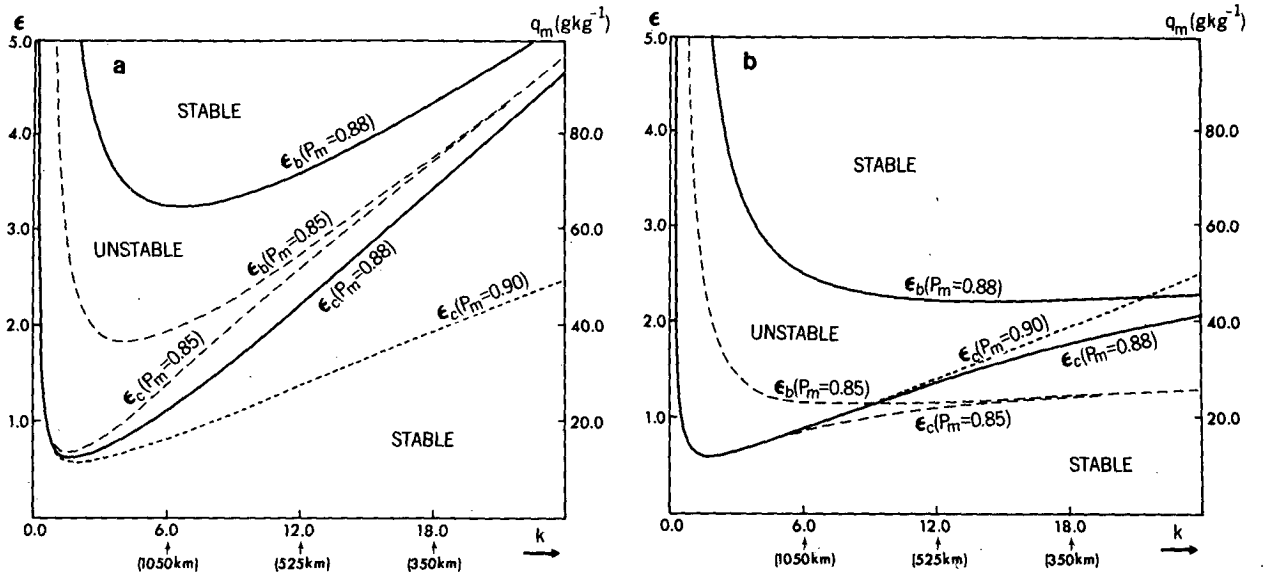

FIG. 3. Schematic instability diagrams for (a) p_m ($=p_b=p_1$) $< p_e$ and (b) p_m ($=p_b$) $< p_e$ ($=p_1$). The top and bottom solid (dashed) curves represent the blowup and neutral modes for $p_m = 0.88$ ($p_m = 0.85$). The dotted curves denote neutral curves for the case where $p_m = p_e = 0.90$. ϵ is the heating intensity coefficient defined by (2.5b). The k and q_m are the nondimensional wavenumber and specific humidity of the moist convergence layer, respectively. All other parameters are given in Table 2.

$p_m = p_b = p_1 = 0.88$. Also shown by dashed curves in Fig. 3a are these modes for $p_m = p_b = p_1 = 0.85$. The region between the blowup and the neutral curves denotes the unstable CISK mode for which the growth rate is positive; all other regions, namely, the regions above the blowup curve and below the neutral curve, represent stable modes for which the growth rates are negative. As a comparison, the neutral curve, ϵ_c, for $p_m = p_e = 0.90$ is also plotted by the short-dashed curve. For fixed wavenumber, the instability threshold, ϵ_c, increases, while the blowup threshold, ϵ_b, decreases as p_m decreases, especially for short waves. As a result, the unstable region shrinks as p_m decreases. Note that, although both the neutral and blowup curves vary when the vertical heating distribution and/or basic state stratification changes, this property remains valid.

Figure 3b outlines the instability diagram for the case where p_m ($=p_b$) $< p_e$ ($=p_1$). The same model parameters were used as used in Fig. 3a, except the parameter p_1. Because $p_1 > p_b$, there is a diabatic heating at the level p_b, i.e., $\eta(p_b) > 0$. We anticipate that, based upon the results of the previous subsection, the CISK modes with short wavelength should be destabilized by the diabatic heating at p_b. In fact, the instability threshold, ϵ_c, is reduced as p_m (or p_b) decreases, and both the blowup and neutral modes tend to appear for much weaker heating intensities at small wavenumbers. However, qualitative similarity between Fig. 3a and Fig. 3b is evident in the sense that the unstable region shrinks with increasing $p_e - p_m$.

From the solution, (A6) given in the Appendix we see that, when the top of the moist layer is located above the cloud base, i.e., $p_m < p_b$ ($p_b \geq p_e$), a singularity of the same nature as was found in (3.6) exists, which makes the growth rate approach infinity at a certain *intermediate* wavelength. One feature is common to both of the cases, $p_m < p_e$ and $p_m < p_b$, namely, that the low-level moisture convergence measured by $\omega(p_m)$ is directly affected by the cumulus heating. Once the heating intensity becomes large enough, the low-level large-scale moisture convergence will be dominated by diabatic heating instead of the Ekman pumping. The larger the value of $p_e - p_m$, the more strongly $\omega(p_m)$ will be controlled by the latent heat and thus the smaller the value of the blowup threshold, ϵ_b; this is demonstrated in Fig. 3a and Fig. 3b. In a previous study of baroclinic wave-CISK (Wang and Barcilon, 1986), it was found that, if the vertical velocity, $\omega(p_m)$, used in the heating representation is induced by the baroclinic forcing below or at cloud base, the solution is well behaved; so long as p_m is above the cloud base value, p_b, the growth rate blows up at some intermediate wavelength. Its origin is basically the same as shown here.

c. *The role of the Earth's rotation and relative vorticity*

The deficiency of the CISK model in producing blowup modes leads one to conclude that in a feasible CISK mechanism the dominant feedback of the cumulus heating on the low-level moisture convergence must be an *indirect* one, in which the Earth's rotation plays an essential part. This mechanism may be briefly summarized as follows. In an atmospheric region with a deep conditionally unstable layer, the low-level con-

vergence associated with some preexisting large-scale disturbance and enhanced by surface friction lifts air parcels to their condensation level and initiates cumulus convection. Release of latent heat in a large number of cumulus towers and cumulonimbi gives rise to a large-scale solinoidal field that induces a thermally driven secondary circulation that is characterized by upper-level divergence and low-level convergence. During this process, eddy available potential energy is generated and partially converted to the eddy kinetic energy of the divergent component of the wind (hereafter referred to as divergent kinetic energy and denoted by K_χ). Notice that the heating-induced low-level convergence can have a direct feedback on the low-level moisture supply, and this completes a direct coupling between the latent heating and the large-scale moisture supply. On the other hand, if the Coriolis force is sufficiently strong, the secondary circulation will be deflected, resulting in a large-scale cyclonic circulation in the lower troposphere and an anticyclonic circulation aloft. In the presence of turbulent friction, the intensified cyclonic *rotational flow* further promotes the horizontal moisture convergence in the boundary layer, which initiates new convection. This completes an indirect coupling between the heating and the moisture supply. Mak's (1981) results, which are derived from a two-level model, show that the blowup mode arose from the part of the heating representation that is directly related to the divergent component of the flow. The results obtained in the previous subsections suggest that the presence of the direct coupling is a necessary but not sufficient condition for the short-wave blowup. The unbounded growth rate at the short wavelengths occurs only when direct coupling dominates over indirect coupling. It is suggested that for a feasible CISK mechanism indirect coupling must dominate over direct coupling, thus the presence of a sufficiently strong Coriolis force is essential.

The energetic analysis in a nonlinear model indicates that the eddy available potential energy cannot be converted directly to the kinetic energy of the rotational component of the wind (hereafter referred to as rotational kinetic energy and denoted by K_ψ). It is the interaction between vorticity and divergence fields that converts the divergent kinetic energy to the rotational kinetic energy (Zeng, 1979). The conversion from the divergent kinetic energy to the rotational kinetic energy can be written as

$$\langle K_\psi K_\chi \rangle = \overline{(f_0 + \nabla^2\psi)(\nabla\psi\nabla\chi)}, \qquad (4.8)$$

where the overbar implies a volume average and ψ and χ are the streamfunction and velocity potential, respectively, i.e.,

$$\mathbf{v}_\psi = \mathbf{k}\times\nabla\psi, \quad \mathbf{v}_\chi = -\nabla\chi, \quad \mathbf{v} = \mathbf{v}_\psi + \mathbf{v}_\chi.$$

It is important to note that an efficient conversion from K_χ to K_ψ requires a sufficiently large planetary vorticity and/or relative vorticity. Therefore, the role of the planetary vorticity, f_0, is of primary importance in spinning up a rotational vortex in the incipient stage when the relative vorticity is weak. In addition to this latitude requirement, a stronger preexisting relative vorticity ($\nabla^2\psi$) also favors development of CISK disturbance.

When the parameterized heating is dominantly controlled by the moisture convergence due to the Ekman pumping, it has been found that, for fixed stratification, $S(p)$, and heating function, $\eta(p)$, the wavelength of the fastest growing mode is proportional to the *inverse* of the Coriolis parameter (see Table 3); i.e., the ratio of the preferred wavelength to the Rossby radius of deformation (defined as $S_0^{1/2}P_0/f_0$) remains constant when the Coriolis parameter varies. The growth rate of the fastest growing mode increases with increasing latitude and is proportional to the *square root* of the Coriolis parameter (see Table 3).

d. *Response of the scale selection to the heating distribution*

Shown in Table 4 is the response of the CISK solution to changes in the position of the maximum heating (a = 0.0, 0.5, 1.0). Since short waves are confined to the lower troposphere, a smaller static stability parameter or stronger heating in the lower troposphere (a = 1) leads to a shorter preferred wavelength. This may explain why the short-wave cutoff crucially depends on the heating condition at the top of the Ekman layer. When comparing the results in Table 4 with those reported by Mak (1983), one finds that the sensitivity of the instability to the vertical distribution of heating is effectively suppressed by the presence of vertical shear in the basic state. It is also obvious from Table 4 that the growth rate estimated by using a Boussinesq model (SP1) is substantially larger than that by a non-Boussinesq model, if the static stability parameter is the same at the surface.

To assess the influence of the heating condition at the top of the Ekman layer, particular calculations have been carried out by changing parameter p_T^* from 850

TABLE 3. The growth rate in day^{-1} and the wavelength in km (given by the numbers in parentheses) of the most unstable CISK mode for different stratification and Coriolis parameter, showing the effect of the Earth's rotation. The parameter a is set to 0.5, and the lapse rate in SP3 is 6°C km^{-1}. The rest of the parameters are the same as used in the reference run.

Stratifications $S(p)$	Coriolis parameter f_0 (s^{-1})		
	0.377×10^{-4} (15°N)	0.50×10^{-4} (20°N)	0.80×10^{-4} (33.4°N)
SP2 $S = S_0/p^2$	0.15 (3800)	0.18 (2880)	0.23 (1800)
SP3 $S = S_0/p^{2-m}$	0.21 (3500)	0.25 (2650)	0.31 (1650)

TABLE 4. Growth rate in day^{-1} and the wavelength in km (given by the numbers in parentheses) of the fastest growing mode for different locations of the maximum heating described by the shape parameter a and for different stratification profiles. The lapse rate used for SP3 is 6°C km^{-1}. All the other parameters are given in Table 2.

	Shape parameter a		
Stratifications	0.0	0.5	1.0
SP1 $S = S_0$	0.72 (3500)	1.22 (2400)	2.23 (1500)
SP2 $S = S_0/p^2$	−0.05 (7850)	0.15 (3800)	0.75 (1960)
SP3 $S = S_0/p^{2-m}$	−0.02 (7850)	0.21 (3500)	0.84 (1850)

to 950 mb. The results are shown in Table 5. The maximum growth rate (preferred wavelength) exhibits a rapid increase (a sharp decrease) with increasing heating or decreasing cooling at the top of the Ekman layer. When p_t^* is put to 1000 mb, the short-wave cutoff is removed, as predicted by (4.4).

5. The effect of the cumulus momentum mixing on CISK disturbance

For motions at lower latitude and/or motions with relatively small horizontal scale, cumulus momentum mixing may play a non-negligible part in CISK dynamics. In the presence of cumulus momentum mixing, the governing equation for the dynamically large-scale perturbation is given by (2.6). To avoid unnecessary complication and to focus our attention on the qualitative effects of the cumulus friction, we adopt a closure assumption of type 1 and assume that the cloud top and base coincide with the model's upper and lower boundaries respectively, i.e., $p_t = p_u$ and $p_b = p_e = p_m$. We consider a motionless basic state with the model stratification, SP2, and the vertical distribution of heat as described by (3.8). In the present model the profile for the mean cumulus mass flux, $M_c(p)$, needs to be prescribed empirically. Diagnostic profiles for $M_c(p)$ deduced by different authors from different datasets appear to differ from each other (e.g., Yanai et al., 1973; Shapiro and Stevens, 1980; Lee, 1984; Chen, 1985). For the sake of simplicity, we assume a constant rate of cloud mass detrainment from cloud base to cloud top, i.e.,

$$M_c^*(p) = M_0^* \frac{p - p_t}{p_b - p_t}, \tag{5.1}$$

where M_0^* is the dimensional mean cumulus mass flux at the cloud base $p = p_b$, which normally has an order of magnitude of −0.1 Pa s^{-1} (−10^{-3} mb s^{-1}), corresponding to a mean tropospheric heating rate of the order of 5°C day^{-1} or a precipitation rate produced by cumulus clouds of the order of 20 mm day^{-1}. This estimate is close to the values of 4 to 5 mb h^{-1} deduced in the budget studies by Yanai et al. (1973) and Chen (1985).

With the above assumptions and specifications, one can obtain from (2.4) and (2.7a,b) the following eigenvalue problem for the vertical structure of the normal mode, $\Omega(p)$:

$$\sigma\frac{d^2\Omega}{dp^2} - i\mathrm{Ro}k^2S(p)M_c(p)\frac{d\Omega}{dp} + \left[\sigma - 2i\mathrm{Ro}\frac{M_0}{p_b - p_t} + i\mathrm{Ro}\frac{2M_c(p)}{p}\right]k^2S(p)\Omega + \epsilon k^2\Omega_m\left[\left(2i\mathrm{Ro}\frac{M_0}{p_b - p_t} - \sigma\right)\times\frac{\eta(p)}{p} + i\mathrm{Ro}M_c(p)\frac{d}{dp}\left(\frac{\eta}{p}\right)\right] = 0, \tag{5.2}$$

subject to the boundary conditions

$$\Omega = 0, \quad \text{at} \quad p = p_u, \tag{5.3a}$$

$$\Omega\left[\sigma - r\frac{k^2\mathrm{Ro}M_c}{\sigma}\left(S - \epsilon\frac{\eta}{p}\right)\right] + ir\frac{d\Omega}{dp} = 0, \quad \text{at} \quad p = p_e. \tag{5.3b}$$

We cannot hope to find a general analytical solution to (5.2) with (5.3a,b). Since we know the exact solution for its counterpart without cumulus momentum mixing, it is convenient to solve (5.2) and (5.3a,b) by using a shooting method (Langer, 1960).

The growth rates, expressed in day^{-1}, are plotted in Fig. 4 as functions of nondimensional wavenumber, k, for various values of M_0^*. For comparison, the growth rate of the CISK mode without cumulus momentum exchange is shown by a solid curve labeled "$M_0 = 0$." We note that, in the presence of cumulus friction, the lower boundary condition, (5.3b), becomes quadratic in σ and singular when $\sigma = 0$. Figure 4 shows that the two groups of growth rate curves diverge with increasing wavenumber; one corresponds to growing modes and the other to decaying modes. When M_0^* is relatively small (−0.01 Pa s^{-1} and −0.02 Pa s^{-1}), the wavelength (growth rate) of the fastest growing mode is slightly shorter (larger) than those corresponding values for the case with $M_0 = 0$. However, the waves shorter than the "inviscid" short-wave cutoff wavelength (around 1200 km) become amplifying modes

TABLE 5. The growth rate in day^{-1} and the wavelength in km (given in parentheses) of the fastest growing mode for different heating intensities at the top of the Ekman layer described by the shape parameter p_t^* and for different stratification profiles. The lapse rate used in SP3 is 6°C km^{-1}. All the other parameters are given in Table 2.

	Shape parameter P_t^* (mb)		
Stratifications	850	900	950
SP2	0.01 (6300)	0.15 (3800)	0.42 (1900)
SP3	0.05 (5200)	0.21 (3500)	0.50 (1850)

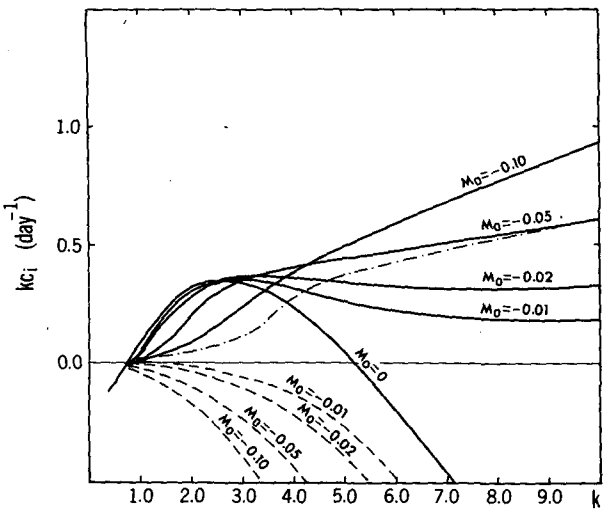

FIG. 4. The growth rate (day^{-1}) as a function of the nondimensional wavenumber k for different cloud mass fluxes at cloud base, M_B^* (in Pa s^{-1}). The solid (dashed) curves represent growing (decaying) CISK mode in the presence of cumulus friction, the dotted–dashed curve denotes the growth rate with constant cloud mass flux, $M^* = -0.05$ Pa s^{-1}.

having growth rates comparable to the maximum value. With increasing cloud mass flux, M_B^* (-0.05 Pa s^{-1} and -0.1 Pa s^{-1}), the instability is suppressed for the waves longer than the "inviscid" preferred wavelength, while considerably enhanced for the shorter waves; thus the shortest wave eventually attains the largest growth rate.

To understand the mechanics responsible for the destabilization (stabilization) of the short (long) waves, we examine the vertical structure of the growing modes for the cases with and without cumulus friction shown in Fig. 5. When there is cumulus friction, the vertical extent of the negative geopotential (or positive vorticity) and positive temperature perturbation is reduced. From the vorticity equation in (2.4), the vorticity source induced by cumulus momentum exchange is

$$VS = \mathrm{Ro}\left[M_c\frac{\partial\zeta}{\partial p} + (\zeta - \zeta_b)\frac{\partial M_c}{\partial p}\right], \qquad (5.4)$$

where the first term is attributed to downgradient vorticity mixing, and the second term expresses the variation of vorticity due to cloud mass detrainment. Notice that both terms are positive near the lower boundary, $p = p_e$, where $\partial\zeta/\partial p < 0$ and $\zeta - \zeta_b > 0$, since $M_c < 0$ and $\partial M_c/\partial p > 0$. This means that the model cumulus friction acts to strengthen positive vorticity at the top of the Ekman layer and to diminish the vertical extent of the CISK disturbances. As a consequence, the generation of eddy available potential energy by diabatic heating, which can be expressed per unit mass at pressure p by $-(\epsilon/S)\eta(p)\overline{\omega(p_m)T(p)}$, takes place in a relatively shallow tropospheric layer near the surface and favors intensification of short waves. In addition, the increase of the relative vorticity at p_e causes more intense Ekman pumping and enhances the low-level moisture convergence. As has been pointed out in section 4, a predominant control over the low-level moisture convergence by diabatic heating (via vertical momentum mixing) would result in a monotonic increase of the growth rate with increasing wavenumber. We should, however, deemphasize this extreme circumstance because the quasi-balance assumption is not valid for very short waves. On the other hand, the model cumulus momentum mixing tends to weaken the anticyclonic circulation aloft and hence to compensate the diabatic heating effect and to suppress the amplification of long waves that extend into the upper troposphere. The dotted–dashed curve in Fig. 4 illustrates the growth rate for the case with a constant cloud mass flux, i.e., $M^*(p) = M_B^* = -0.05$ Pa s^{-1}. In this case, the dissipative effect of cumulus friction is more significant at long wavelengths; the growth of these longer waves is seen to be reduced substantially.

6. Concluding remarks

Regardless of the fundamental difficulties in interpreting the growth of tropical storms, the basic idea of CISK remains valuable in understanding the interaction between cumulus convection and large-scale disturbances. It appears to be particularly relevant in explaining the development of some extratropical and subtropical weather systems for which the convective heating is a primary driving force. Using a generalized solution for a continuous CISK model, we have examined the behaviors of CISK under two different closure assumptions.

The first assumes that the amount of latent heat released by moist convection in a vertical column is proportional to the supply of moist air at the top of the Ekman boundary layer (Ooyama, 1964, 1969). Under this assumption, the CISK solution exhibits scale selection and short-wave cutoff if no latent heat is released at the top of the boundary layer, p_e (Fig. 2). When the convective heating is present at p_e, the large-scale moisture convergence at the top of boundary layer is controlled by both the convective heating and the Ekman pumping [see (4.5)]; therefore, the instability behavior at the shortest wavelength crucially depends upon the competition between the convective heating in situ and the Ekman pumping-induced cooling. If the former exceeds the latter, the growth rate increases monotonically with decreasing wavelength. On the other hand, when the criterion for short-wave blowup, (4.4), is not satisfied, the short-wave cutoff is generally present but not necessarily warranted (Wang, 1987b). The presence of short-wave cutoff and wave selection requires that the CISK threshold, ϵ_c, defined by (4.3) possesses a minimum at an intermediate wavelength.

The second closure assumption assumes that the amount of latent heating is proportional to the moisture

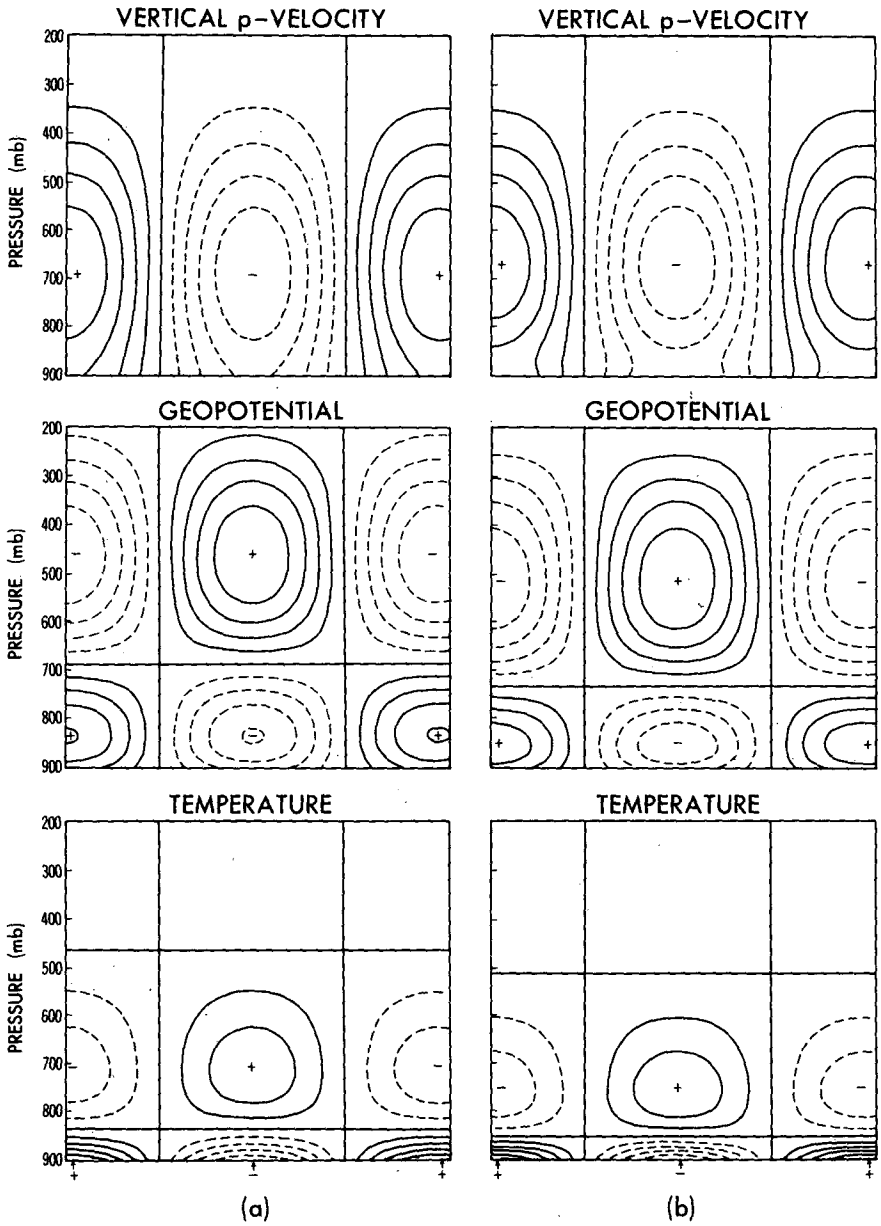

FIG. 5. Vertical structures of the CISK modes: (a) for the case where $M_0^* = 0$ and at $k = 2.65$ (the most unstable wave) and (b) for the case where $M_0^* = -0.05$ Pa s^{-1}. All other parameters are the same as used for the reference run (Table 2) except $p_u = p_t = 200$ mb. Contour plots for the nondimensional geopotential height, temperature and vertical p-velocity are normalized by their maximum values in the domain.

supply at an interior level above the Ekman layer. With this assumption, the growth rate of the CISK perturbation may become infinitely large at a certain middle wavelength as heating intensity reaches a critical value [condition (4.6)].

The unbounded growth rates that occur at the shortest wavelength under closure assumption 1, $p_m = p_e$, and at a middle wavelength under closure assumption 2, $p_m < p_e$, are both associated with a common situation that is characterized by a local warming at the top of the moist convergence layer in the area of rising motion. In this circumstance, the low-level water vapor convergence sustaining the cumulus heating is directly controlled by the heating itself, and the divergent component of wind will be no longer negligible compared to the rotational component once heating becomes strong enough. Therefore, the balance or quasi-geostrophic assumption breaks down before the CISK

mode acquires infinitely large growth. This situation also contradicts the underlying hypothesis of the CISK theory that the cumulus convection cannot, by itself, maintain the low-level convergence necessary for the maintenance of cumulus clouds. It is suggested that in a viable CISK mechanism the *dominant* feedback of the convective heating to the large-scale moisture convergence must be of an *indirect* nature. A quantitative indicator of this necessary condition is the absence of warming at the level where the vertical velocity is used for the heating representation.

The efficient conversion of the heating-induced divergent kinetic energy into the rotational kinetic energy, or the spinup of a dynamically large-scale vortex, requires a sufficiently large value of the planetary vorticity (f) and/or a significant preexisting relative vorticity. For a representative model stratification and heating distribution, it is found that the growth rate of the fastest growing mode is proportional to the square root of the Coriolis parameter, and the preferred wavelength is proportional to the inverse of the Coriolis parameter. In our view, a sufficiently strong Coriolis force is not only necessary for the maintenance of a dynamically large-scale system for which the rotational flow is dominant, but is also required if a large-scale system is to respond to the convective heating by adjusting its rotational component of the motion. The balance or quasi-geostrophic assumption would ensure such a strength of the Coriolis force. In this sense, the balance assumption is an indispensible part of the CISK mechanism.

In the absence of cumulus friction, the linear CISK model possesses a unique unstable mode. When cumulus momentum mixing is included, *two* solutions are found in the model; one is amplifying and the other decaying. The model cumulus momentum exchange plays a dual role in CISK dynamics. On the one hand, it tends to strengthen the cyclonic circulation and the ascending motion at the top of the Ekman layer and to reduce the vertical extent of the disturbance; as a consequence, the release of latent heat is enhanced and short waves are destabilized dramatically. On the other hand, the vertical momentum mixing weakens anticyclonic circulation aloft, so that long waves are dissipated or stabilized. Results from diagnostic studies have shown that cumulus momentum mixing mainly reduces the positive vorticity in the middle troposphere and the negative vorticity in the upper levels, but does not appreciably alter the vorticity at the top of planetary boundary layer (e.g., Tollerud and Esbensen, 1983; Sui and Yanai, 1986). The present representation of vertical cumulus momentum exchange seems to exaggerate its contribution to latent heat release by increasing cyclonic vorticity at the top of the Ekman layer. At the same time, it also underestimates its dissipation on the perturbation vorticity because of the assumption of a mean cloud mass detrainment which rapidly decreases with height. Besides, the mean cloud mass detrainment, $M_d(p)$, and the heating distribution function, $\eta(p)$, are not entirely independent of each other. Both of them should be determined by cloud dynamics and physics. A more reasonable description of the cumulus momentum mixing is apparently needed.

Acknowledgments. The comments from Dr. Ooyama and anonymous reviewers are very helpful in clarifying the presentation of this work, in particular, the issue of the applicability of linear CISK to real atmospheric phenomena. I wish to express my appreciation to Drs. Y. Kurihara, I. Orlanski, N. Crook and B. B. Ross for reading and commenting on an early draft of the manuscript. I thank Mrs. Callan for typing the manuscript and the GFDL drafting group for preparing the figures. This work was supported by NOAA/Princeton University Grant NA84EAD00057.

APPENDIX

CISK Solution for the Case When $p_m < p_b$

According to Wang and Barcilon (1986), when $p_m < p_b$ the dispersion relation can be expressed as

$$f_1(p_u) - \epsilon k^2[I + f_1(p_m)I_2(p_b)] = 0, \tag{A1}$$

where f_1 and I_2 are defined by (3.3) and (3.4), respectively. The quantity, I, resulting from the direct feedback of the cumulus heating on the low-level convergence, can be written as

$$I = f_2(p_m)[I_1(p_b) - I_1(p_m)] - f_1(p_m)[I_2(p_b) - I_2(p_m)], \tag{A2}$$

where

$$f_2(p) \equiv \Omega_1(p_u)\Omega_2(p) - \Omega_2(p_u)\Omega_1(p), \tag{A3}$$

$$I_1(p) \equiv \sigma C(p) + irD(p). \tag{A4}$$

$C(p)$ and $D(p)$ have the following definitions:

$$C(p) = \int_{P_t}^{P} \frac{\eta(t)}{t} \frac{[\Omega_1(p_e)\Omega_2(t) - \Omega_2(p_e)\Omega_1(t)]}{[\Omega_1'(t)\Omega_2(t) - \Omega_2'(t)\Omega_1(t)]}\,dt, \tag{A5a}$$

$$D(p) = \int_{P_t}^{P} \frac{\eta(t)}{t} \frac{[\Omega_1'(p_e)\Omega_2(t) - \Omega_2'(p_e)\Omega_1(t)]}{\Omega_1'(t)\Omega_2(t) - \Omega_2'(t)\Omega_1(t)}\,dt. \tag{A5b}$$

From (A1) through (A4), we obtain

$$\sigma = ir \frac{\epsilon k^2\{f_2(p_m)[D(p_b) - D(p_m)] - B(p_m)I_2(p_m)\} - B(p_u)}{A(p_u) - \epsilon k^2\{f_2(p_m)[C(p_b) - C(p_m)] + A(p_m)I_2(p_m)\}}. \tag{A6}$$

REFERENCES

Bannon, P. R., 1986: Linear development of quasi-geostrophic baroclinic disturbances with condensational heating. *J. Atmos. Sci.*, **43**, 2261–2274.

Chang, C. P., and R. T. Williams, 1974: On the short-wave cutoff of CISK. *J. Atmos. Sci.*, **31**, 830–833.

Charney, J. G., 1973: Movable CISK. *J. Atmos. Sci.*, **30**, 50–52.

——, and A. Eliassen, 1949: A numerical method for predicting the

perturbations of the middle-latitude westerlies. *Tellus,* **1,** 38–54.

——, and ——, 1964: On the growth of the hurricane depression. *J. Atmos. Sci.,* **21,** 68–75.

Chen, S.-J., and L. D. Dell'Osso, 1984: Numerical prediction of the heavy rainfall vortex over Eastern Asia monsoon region. *J. Meteor. Soc. Japan,* **62,** 730–747.

Chen, Y-L., 1985: Diagnosis of net cloud mass flux in GATE. *J. Atmos. Sci.,* **42,** 1757–1769.

Davies, H. C., and de Guzman, R. A., 1979: On the preferred mode of Ekman-CISK. *Tellus,* **31,** 406–412.

Dell'Osso, L. D., and S.-J. Chen, 1986: Numerical experiments on the genesis of vortices over the Qinghai–Tibet plateau. *Tellus,* **38A,** 236–250.

Emanuel, K. A., 1983: Elementary aspects of the interaction between cumulus convection and the large-scale environment. *Mesoscale Meteorology—Theories, Observations and Models,* D. K. Lilly and T. Gal-chen, Eds. D. Reidel, 551–575.

——, 1986: An air–sea interaction theory for tropical cyclones. Part I: steady-state maintenance. *J. Atmos. Sci.,* **43,** 586–604.

Gyakum, J. R., 1983: On the evolution of the QEII storm. II: Dynamic and thermodynamic structure. *Mon. Wea. Rev.,* **111,** 1156–1173.

Johnson, R. H., 1984: Partitioning tropical heat and moisture budgets into cumulus and mesoscale components: Implications for cumulus parameterization. *Mon. Wea. Rev.,* **112,** 1590–1601.

Koss, W. J., 1976: Linear stability of CISK-induced disturbances: Fourier component eigenvalues analysis. *J. Atmos. Sci.,* **33,** 1195–1222.

Krishnamurti, T. N., M. Kanamitsu, R. Godbole, C. B. Chang, F. Carr and J. H. Chow, 1976: Study of a monsoon depression (II), Dynamic structure. *J. Meteor. Soc. Japan,* **54,** 208–224.

Kuo, H.-L., 1974: Further studies of the parameterization of the influence of cumulus convection on large-scale flow. *J. Atmos. Sci.,* **31,** 1231–1240.

Langer, R. E., 1960: *Boundary Problems in Differential Equations.* The University of Wisconsin Press, 324 pp.

Lee, C-S., 1984: The bulk effects of cumulus momentum transports in tropical cyclones. *J. Atmos. Sci.,* **41,** 590–603.

Lu, J.-N., Z.-A. Qian, F.-M. Shan, Y.-X. Cai and Y.-C. Chen, 1984: Composite structure of summer Qinghai–Xizang Plateau low vortices. *Collected Works of QXPMEX (II),* Science Press, 195–205 (in Chinese).

Mak, M., 1981: An inquiry on the nature of CISK. Part I. *Tellus,* **33,** 531–537.

——, 1982: On moist baroclinic instability. *J. Atmos. Sci.,* **39,** 2028–2037.

——, 1983: On moist quasi-geostrophic baroclinic instability in a general model. *Sci. Sin.,* **B26,** 850–864.

Moorthi, S., and A. Arakawa, 1985: Baroclinic instability with cumulus heating. *J. Atmos. Sci.,* **42,** 2007–2031.

Ooyama, K., 1964: A dynamic model for the study of tropical cyclone development. *Geofis. Int.* (Mexico), **4,** 187–198.

——, 1969: Numerical simulation of the life cycle of tropical cyclones. *J. Atmos. Sci.,* **26,** 3–40.

——, 1971: A theory on parameterization on cumulus convection. *J. Meteor. Soc. Japan,* **49**(special issue), 744–756.

——, 1982: Conceptual evolution of the theory and modeling of the tropical cyclone. *J. Meteor. Soc. Japan,* **60,** 369–379.

Pedersen, T. S., and E. Rasmussen, 1985: On the cut-off problem in linear CISK models. *Tellus,* **37A**(polar low special issue), 394–402.

Rasmussen, E., 1979: The polar low as an extratropical CISK disturbance. *Quart. J. Roy. Meteor. Soc.,* **105,** 531–550.

Rosenthal, S. L., 1978: Numerical simulation of tropical cyclone development with latent heat release by the resolvable scale. I: Model description and preliminary results. *J. Atmos. Sci.,* **35,** 258–271.

Sardie, J. M., and T. T. Warner, 1983: On the mechanism for the development of polar lows. *J. Atmos. Sci.,* **40,** 869–881.

Schneider, E. K., and R. S. Lindzen, 1976: A discussion of the parameterization of momentum exchange by cumulus convection. *J. Geophys. Res.,* **81,** 3158–3160.

Shapiro, L. J., and D. E. Stevens, 1980: Parameterization of convective effects on the momentum and vorticity budgets of synoptic scale Atlantic tropical waves. *Mon. Wea. Rev.,* **108,** 1816–1826.

Smith, P. J., P. M. Dare and S.-J. Lin, 1984: The impact of latent heat release on synoptic scale vertical motions and the development of extratropical cyclone system. *Mon. Wea. Rev.,* **112,** 2421–2430.

Stevens, D. E., and R. S. Lindzen, 1978: Tropical wave-CISK with a moisture budget and cumulus friction. *J. Atmos. Sci.,* **35,** 940–961.

——, R. S. Lindzen and L. J. Shapiro, 1977: A new model of tropical waves incorporating momentum mixing by cumulus convection. *Dyn. Atmos. Oceans.,* **1,** 365–425.

Sui, C-H., and M. Yanai, 1986: Cumulus ensemble effects on the large scale vorticity and momentum fields of GATE. Part I: Observational evidence. *J. Atmos. Sci.,* **43,** 1618–1642.

Syōno, S., and M. Yamasaki, 1966. Stability of symmetrical motions driven by latent heat release by cumulus convection under the existence of surface friction. *J. Meteor. Soc. Japan,* **44,** 353–375.

Tollerud, E. I., and S. K. Esbensen, 1983: An observational study of the upper-tropospheric vorticity fields in GATE cloud clusters. *Mon. Wea. Rev.,* **111,** 2161–2175.

Tracton, M. S., 1973: The role of cumulus convection in the development of extratropical cyclones. *Mon. Wea. Rev.,* **101,** 573–593.

Wang, B., 1987a: On the development mechanism for Tibetan Plateau warm vortices. Submitted to *J. Atmos. Sci.*

——, 1987b: Another look at CISK in polar oceanic air masses. *Tellus* (in press).

——, and A. Barcilon, 1986: Moist stability of a baroclinic zonal flow with conditionally unstable stratification. *J. Atmos. Sci.,* **43,** 705–719.

——, and I. Orlanski, 1987: Study of a heavy rain vortex formed over the eastern flank of the Tibetan Plateau. *Mon. Wea. Rev.* (in press).

Yanai, M., S. Esbensen and J. H. Chu, 1973: Determination of bulk properties of tropical cloud clusters from large-scale heat and moisture budgets. *J. Atmos. Sci.,* **30,** 611–627.

Yeh, T. C., 1979: Summary. *The Qinghai–Xizang (Tibet) Plateau Meteorology,* T. C. Yeh and Y. X. Gao, Eds. Science Press, 267–275 (in Chinese).

Zeng, Q.-C., 1979: *The Mathematical and Physical Foundation for Numerical Weather Prediction.* Science Press, 59–64 (in Chinese).